Science Advances
AAAS

advances.sciencemag.org/cgi/content/full/5/5/eaav5003/DC1

Supplementary Materials for

Carbon doping of WS_2 monolayers: Bandgap reduction and p-type doping transport

Fu Zhang, Yanfu Lu, Daniel S. Schulman, Tianyi Zhang, Kazunori Fujisawa, Zhong Lin, Yu Lei, Ana Laura Elias, Saptarshi Das*, Susan B. Sinnott*, Mauricio Terrones*

*Corresponding author. Email: mut11@psu.edu (M.T.); sbs5563@psu.edu (S.B.S.); sud70@psu.edu (S.D.)

Published 24 May 2019, *Sci. Adv.* **5**, eaav5003 (2019)
DOI: 10.1126/sciadv.aav5003

This PDF file includes:

Supplementary Materials

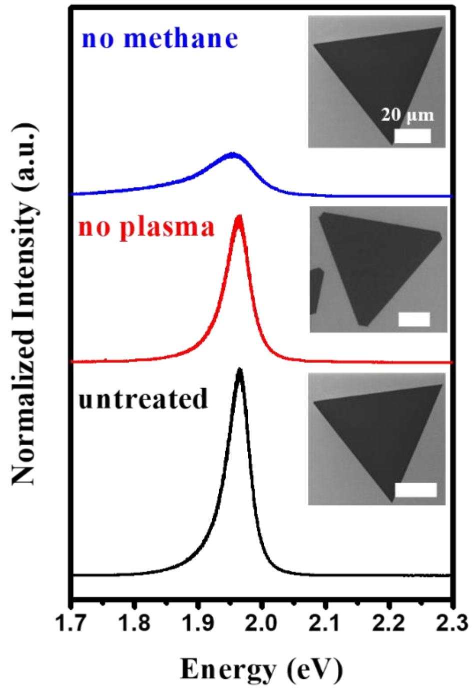

Fig. S1. PL responses of reference samples. Pristine WS_2 (bottom), WS_2 annealed at 400^{o}C in a CH_4 environment (middle), and Ar/H_2 plasma treated WS_2 in the absence of CH_4 (top). As CH_4 cannot be thermally decomposed at 400^{o}C in the absence of plasma, the spectra from heat treated and pristine samples are very similar. Ar/H_2 plasma treatment (without CH_4) causes sulfur atoms to be sputtered away from WS_2, therefore the top panel shows both a quenching and a defect related shoulder in the PL response, as expected. In all panels, insets exhibit the corresponding scanning electron microscopy (SEM) images of the WS_2, showing no morphology changes among these three different samples.

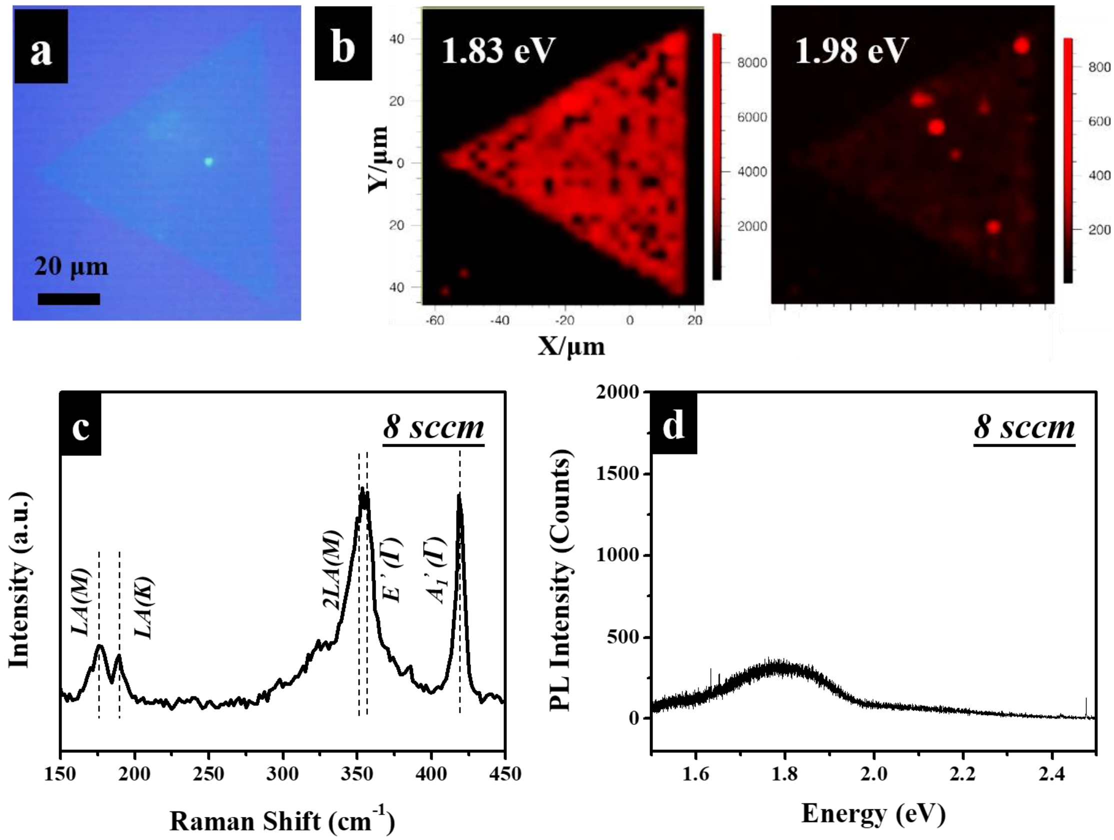

Fig. S2. PL mapping of carbon-doped WS_2, Raman and PL of heavily carbon-doped WS_2. (a) and (b) show the uniformity of the PL of the carbon-doped WS_2 @ 5sccm, measured with a 488 nm laser. (a) Optical image of a WS_2 triangular monolayer. (b) PL mappings showing the intensity of the response at 1.83 eV and 1.98eV, respectively. The mapping at 1.83 exhibits a mostly uniform PL signal, with the exception a few areas with local structural defects (such as holes in the triangles) or undoped parts (that emit at 1.98 eV). **(c) Raman and (d) PL of heavily-carbon-doped WS_2 (@ 8sccm).** Extra carbon doping may result in severe PL quenching but the characteristic Raman signatures of WS_2 are preserved.

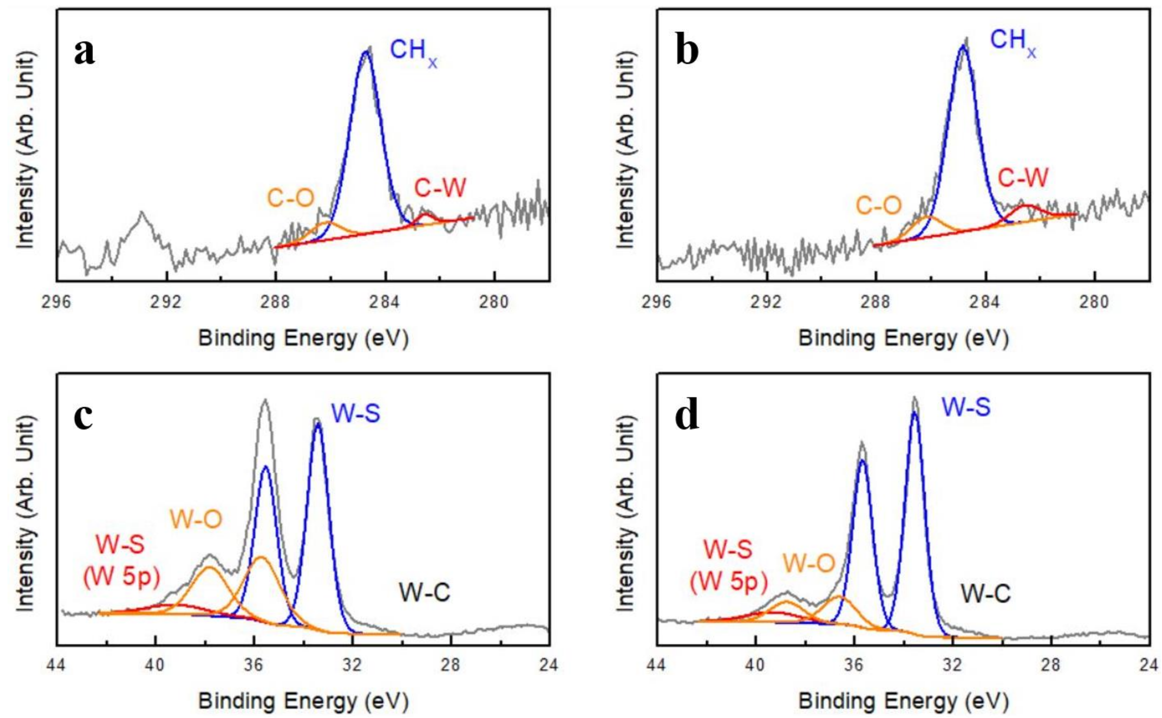

at. %	Si	O	S	W as WS_2	W as WO_3	C	C as W-C	C in WS_2
Pristine	23.5	50.0	11.1	4.9	2.1	8.0	0.22	1.98
Doped	21.9	43.2	15.0	8.0	1.3	10.4	0.80	5.33

Fig. S3. XPS analyses of the carbon-doped WS_2. X-ray photoelectron spectroscopy (XPS) elemental analyses of pristine WS_2 (a) C 1s, (c) W 4f, and carbon-doped WS_2 (b) C 1s and (d) W 4f core levels. The table list shows elemental compositions in both the pristine and carbon-doped WS_2. The carbon exists on the material surface mostly in the form of CH_X and CO_X (intense peak centered at ~ 284.8 eV). The C 1s line scans show that the carbon in the form of carbide bonding (red curve at around 282.5 eV) increased three times after doping, which indicates the formation of the new W-C bonds that substitute sulfur atoms in the WS_2 lattice. We have also characterized and compared the pristine WS_2 and carbon-doped WS_2 samples by ToF-SIMS (Time of Flight Secondary Ion Mass Spectrometry), and FTIR (Fourier Transform Infrared Spectroscopy). The low signal to noise ratio lead to difficulties in detecting the characteristic features from doped carbon species.

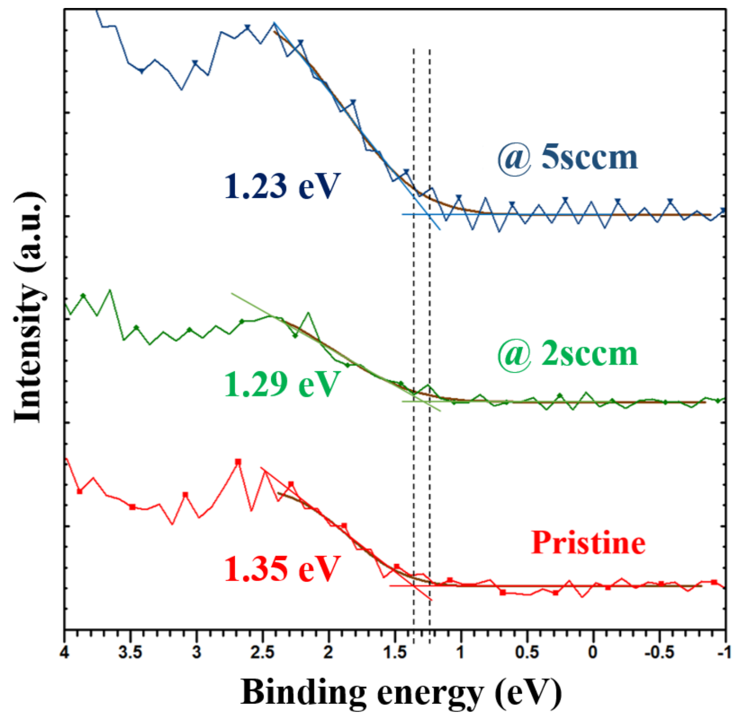

Fig. S4. VBM of the carbon-doped WS_2. The carbon incorporation into WS_2 gradually saturates the sulfur vacancies, thus decreasing the energy of the valence band maximum (VBM) to the Fermi level (FL), as shown in the figure, from 1.35 eV (pristine) to 1.29 eV (doped @2 sccm) and 1.23 eV (doped @5 sccm). All three spectra show similar valence band signatures of WS_2 that indicate that the binding energy shift was induced by carbon doping in WS_2.

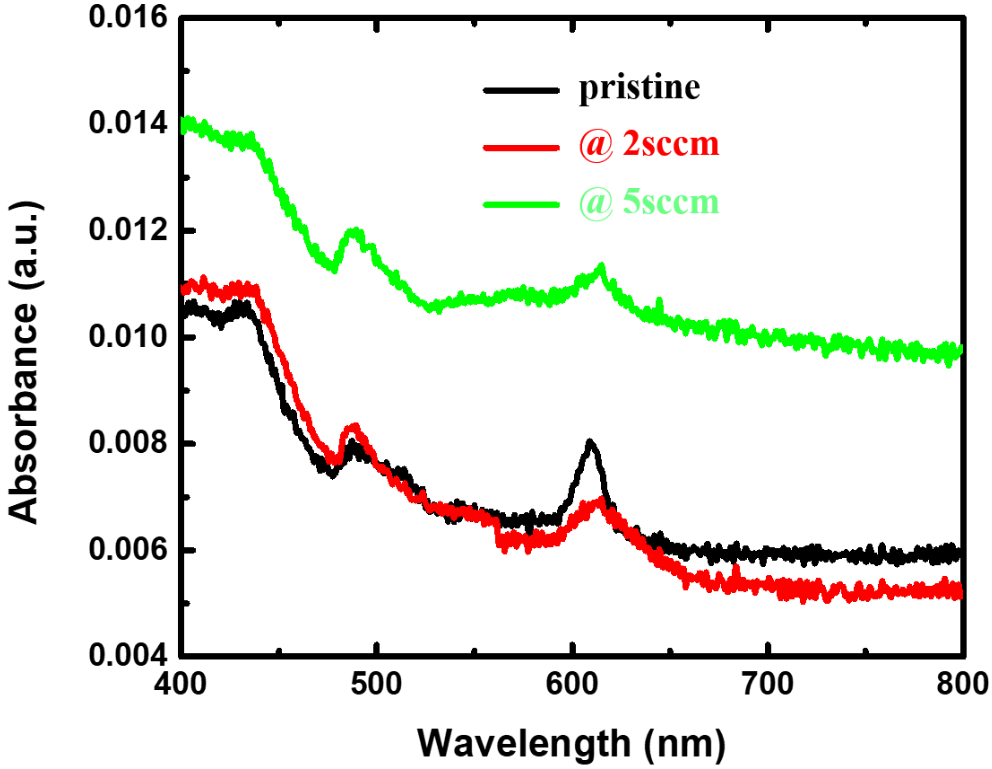

Fig. S5. UV-Vis spectra of the carbon-doped WS_2. The A exciton can be observed at 608 nm (2.039 eV) in the as grown WS_2, which corresponds to the excitonic absorption at the K point of the Brillouin zone. This is one of the characteristic absorption peaks of the monolayered WS_2. As the percentage of C in WS_2 increases, the A excitonic transition gradually shifts from 2.039 eV (608 nm) to 2.020 eV (614 nm) in lightly-doped WS_2 (@2 sccm), and 2.016 eV (615 nm) in medium-doped WS_2(@5 sccm). The red shifts in the A excitonic transitions further support the bandgap reduction via C doping.

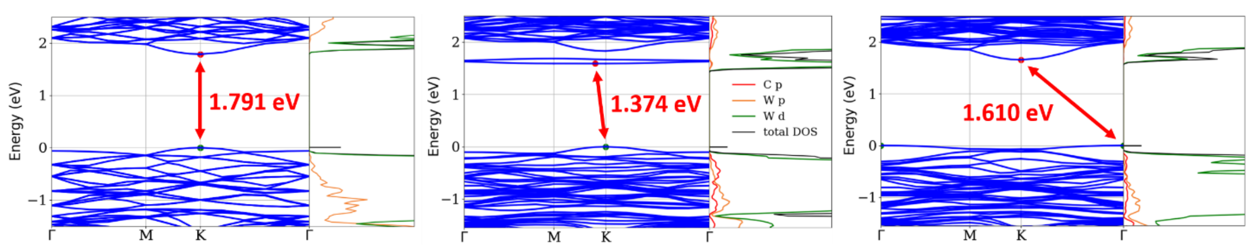

Fig. S6. Complementary band structures and DOS of monolayer pristine WS_2 and carbon-doped WS_2. Band structure and density of states (DOS) of (a) monolayer pristine WS_2, (b) carbon-doped WS_2 with CH_2 units bonded at the β position of the single sulfur vacancy, and (c) CH_2-doped WS_2 with the dopant at the α position. In the DOS, p-orbitals of C and W atoms, d-orbital of W atoms, and total DOS are plotted in different colors.

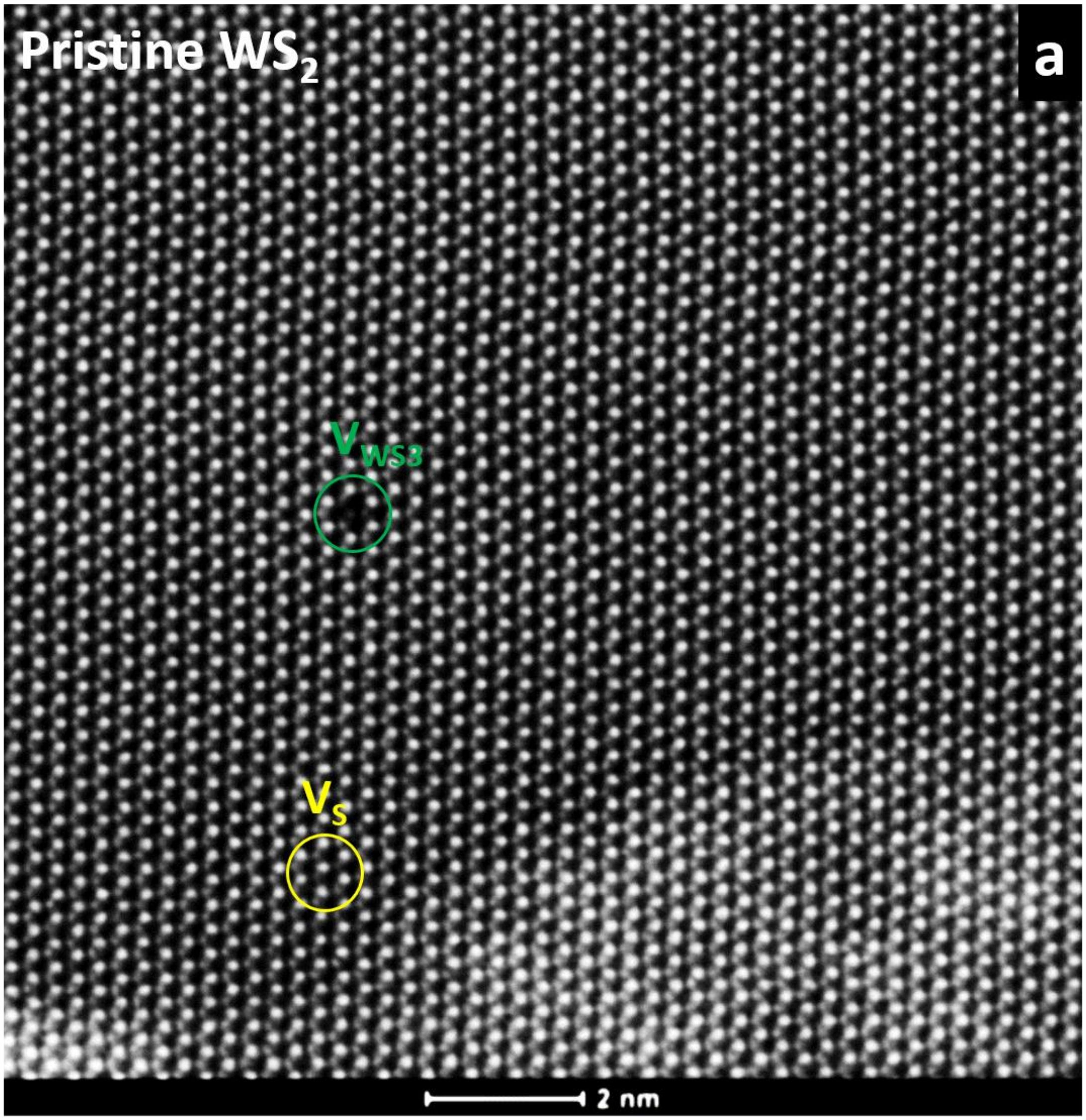

Pristine WS$_2$
a
V$_{WS3}$
V$_S$
2 nm

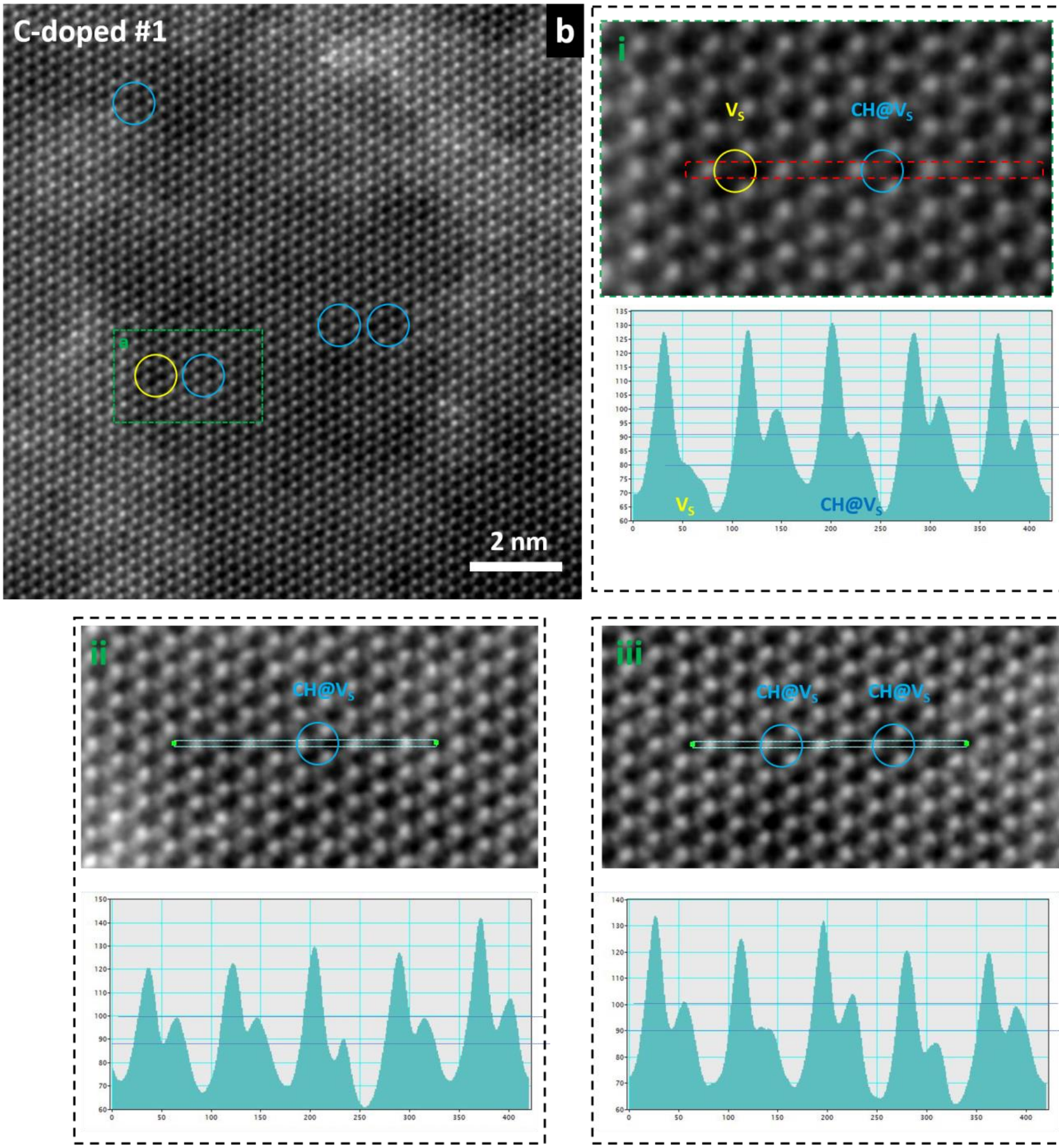

C-doped #1
b
a
2 nm
i
V$_S$
CH@V$_S$
ii
CH@V$_S$
iii
CH@V$_S$
CH@V$_S$

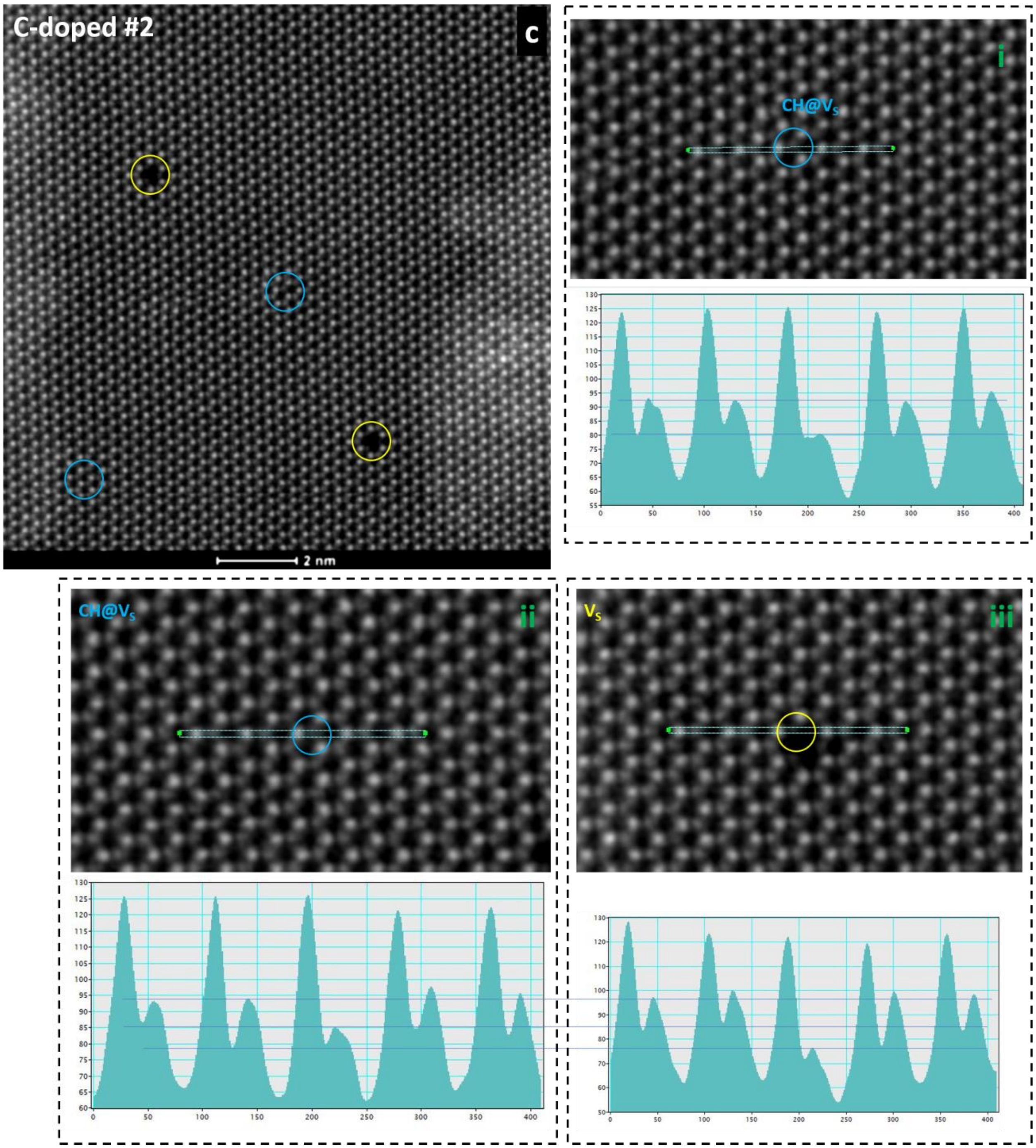

C-doped #2
c
2 nm
i
CH@V$_S$
ii
CH@V$_S$
iii
V$_S$

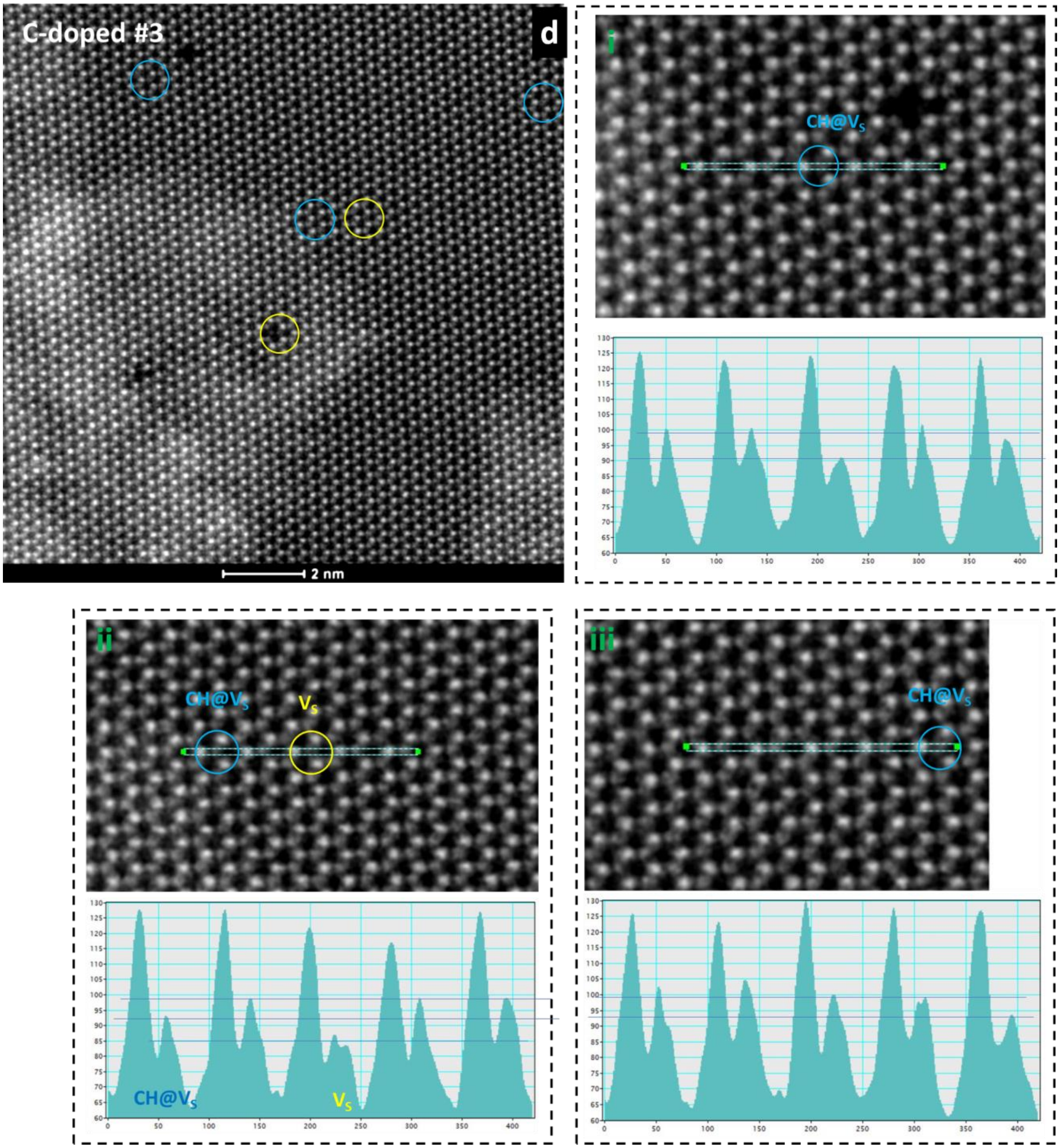

Fig. S7. Experimental STEM examples and identification of sulfur monovacancies and carbon dopant in pristine and carbon-doped WS_2 monolayers. A single sulfur vacancy (Vs) is highlighted with a yellow circle, and tungsten vacancies (V_{WS3}) with green circles. The hexagonal WS_2 lattice can also be identified from the ADF intensity. **Examples of carbon-doped WS_2 monolayers** (b-d) showing the CH@Vs (blue circles) and Vs defects (yellow circles) identified by the ADF image intensity. The line profiles clearly show differences in the intensities when comparing CH@Vs and Vs. We made sure that this intensity profile line-scan avoid the contaminated polymer residue regions by only analyzing atomically clean areas.

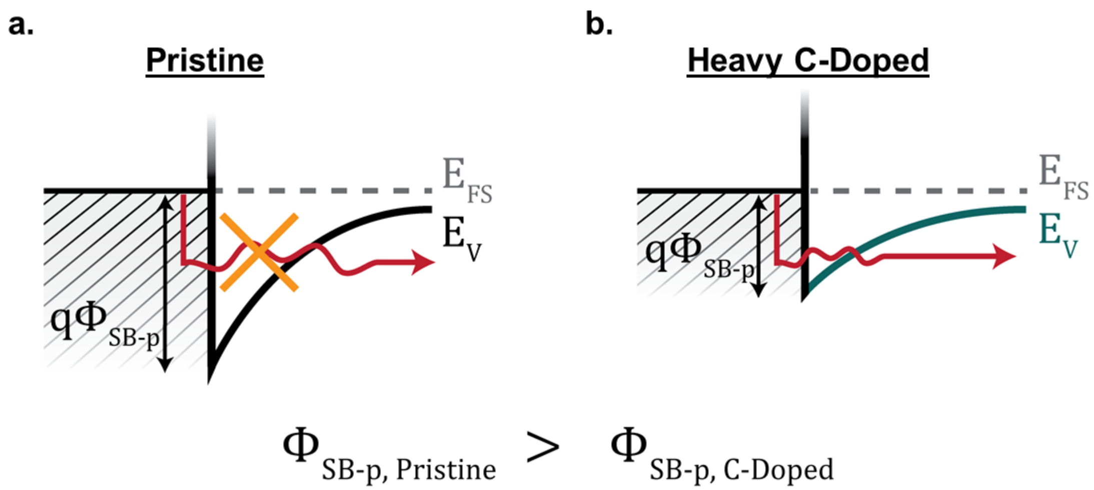

Fig. S8. Band diagram showing the change in Fermi level pinning. Schematic of the valence band position (E_V) near the source for a (a) pristine and (b) carbon-doped FET (@ 8sccm), respectively. For the pristine devices, a tall and wide Schottky tunnel barrier ($\Phi_{SB\text{-}p}$) prevents any hole conduction and hence no p-branch is observed. Conversely, after heavy doping (@ 8sccm), the metal Fermi level pins closer to the WS_2 valence band. Thus, heavily-doped samples have a smaller Schottky barrier height for hole injection and, therefore, exhibit significant hole conduction.

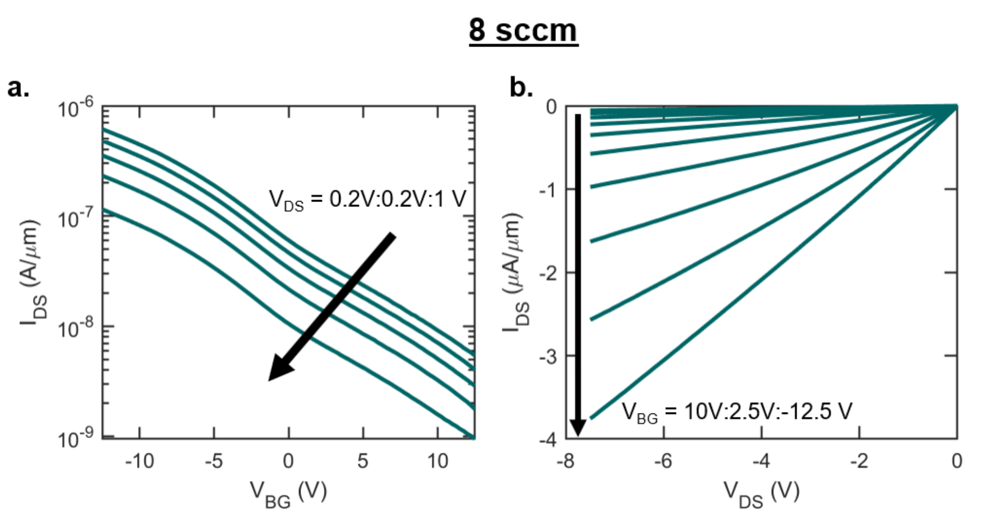

Fig. S9. Transfer and output characteristics of a carbon-doped WS_2–based FET (@8 sccm CH_4). (a) Drain voltage (I_{DS}) versus back gate voltage (V_{BG}) and (b) I_{DS} versus drain voltage (V_{DS}). The device shows heavy p-doping and linear I_{DS} versus V_{DS} characteristics, indicating the metal-WS_2 Fermi level is pinned relatively close to the valence band.

Table S1. Local strain of WS_2 with premade single vacancies and different ligands on C atoms and dopant positions. The local strain is compared to pristine WS_2.

Premade Vacancy Type	Type of Dopant	Strain Compared to Pristine WS_2		
		Doped C Position		
		α	β	γ
Single Vacancy	C	-0.21%	-0.24%	0.50%
	CH	-0.43%	-0.10%	0.53%
	CH_2	-0.32%	-0.11%	0.74%